A Stretched Coordinate Technique for Numerical Absorption of Evanescent and Propagating Waves in Planar Waveguiding Structures

Michael A. Gribbons, William P. Pinello, and Andreas C. Cangellaris, *Member, IEEE*

Abstract—**Berenger's PML technique is modified to allow for the absorption of evanescent and propagating waves in FDTD modeling of wave propagation in planar waveguiding structures. Analytic results illustrate the validity and capability of the proposed modification. Numerical studies explain the numerical implementation of the modified PML in the FDTD and in the compact 2D-FDTD algorithms. Guidelines for the proper selection of the various parameters that govern the performance of the modified PML are presented. The results from simulations indicate that the proposed modified PML grid truncation can be used efficiently for highly accurate numerical analysis of planar waveguiding structures.**

I. Introduction

BERENGER'S PERFECTLY MATCHED layer (PML) approach to the truncation of FDTD grids has been used successfully in conjunction with electromagnetic radiation and scattering problems in two and three dimensions [1]–[3]. An alternative approach to the construction of the PML's directly from Maxwell's equations using stretched coordinates was presented in [4]. However, up to this point there has been no detailed investigation of the performance of PML's with regards to absorption of bound waves with evanescent behavior transverse to their direction of propagation. Except for a brief discussion in [3], there has been no careful investigation of the effect that a PML, positioned parallel to the media interface that supports such bound waves, might have on the propagation characteristics of the wave, especially when the PML is brought close to the interface.

Published results from FDTD simulations of radiation and scattering problems indicate that the PML's can be brought very close (as close as 2 grid cells) to the radiator/scatterer. Such a capability is highly desirable for the FDTD analysis of integrated microwave, millimeter wave and optical circuits, in order to keep computer memory requirements and CPU time at a minimum without sacrificing the numerical accuracy of the simulations. Such circuits include a variety of resonant structures, the electromagnetic behavior of which is dependent on the dispersive propagation characteristics of the waves supported by the waveguiding sections that comprise them. Consequently, it is important to investigate and comprehend the impact of the PML's on the dispersive characteristics of planar waveguiding structures before any circuit-level FDTD simulations using PML's can be performed with confidence.

It is shown in this paper that Berenger's PML truncation scheme is unable to absorb evanescent waves. First, an analytic study of the eigenvalue problem of wave propagation in a dielectric slab waveguide sandwiched between PML's is used to show that, in their original form, Berenger's PML's disturb the characteristics of propagating (bounded) eigenmodes and perturb the values of their effective indices of refraction. Next, a modification to the original PML is introduced to alleviate this difficulty. The proposed modified PML is then implemented in the numerical simulation of wave propagation in slab waveguides. These simulations are used to describe the numerical implementation of the modified PML in the FDTD algorithm and demonstrate its validity and numerical performance. Finally, applications of the modified PML in the compact 2D-FDTD dispersion analysis of open microstrip structures are presented. These applications are used to study the impact of the various modified PML parameters (e.g., distance from waveguides, PML thickness, etc.) on the absorption performance of the PML, and thus generate guidelines for their proper selection.

II. Theory

Using the stretched coordinate approach proposed in [4], Maxwell's curl equations in a linear, isotropic medium are written as

$$\frac{\partial}{\partial t}\epsilon\vec{E} = \nabla_s \times \vec{H} \tag{1}$$

$$-\frac{\partial}{\partial t}\mu\vec{H} = \nabla_s \times \vec{E} \tag{2}$$

where

$$\nabla_s = \hat{x}\frac{1}{s_x}\frac{\partial}{\partial x} + \hat{y}\frac{1}{s_y}\frac{\partial}{\partial y} + \hat{z}\frac{1}{s_z}\frac{\partial}{\partial z}. \tag{3}$$

We restrict our attention to the two-dimensional case with $\partial/\partial y = 0$. As it is well known, Maxwell's equations decouple into two independent sets, one involving the field components H_y, E_x, and E_z (TM polarization), and one involving the

Manuscript received March 1, 1995; revised July 10, 1995. This work was supported in part by the Advanced Technology Program of the U.S. Department of Commerce through a grant to the National Storage Industry Consortium and by Semiconductor Research Corporation Contract 94-PP-086.

The authors are with the Center for Electronic Packaging Research, Department of Electrical and Computer Engineering, University of Arizona, Tucson, AZ 85721 USA.

IEEE Log Number 9415466.

field components E_y, H_x, and H_z (TE polarization). Assuming time-harmonic variation of the form $\exp(j\omega t)$, where $j = \sqrt{-1}$, the pertinent equations for the TM polarization in a homogeneous medium with constant μ and ϵ are

$$j\omega\epsilon E_{z_x} = \frac{1}{s_x}\frac{\partial}{\partial x}(H_{y_x} + H_{y_z}) = \frac{1}{s_x}\frac{\partial}{\partial x}H_y \tag{4}$$

$$j\omega\epsilon E_{x_z} = -\frac{1}{s_z}\frac{\partial}{\partial z}(H_{y_x} + H_{y_z}) = -\frac{1}{s_z}\frac{\partial}{\partial z}H_y \tag{5}$$

$$j\omega\mu H_{y_x} = \frac{1}{s_x}\frac{\partial}{\partial x}E_{z_x} \tag{6}$$

$$j\omega\mu H_{y_z} = -\frac{1}{s_z}\frac{\partial}{\partial z}E_{x_z} \tag{7}$$

where the split-component formalism used with Berenger's PML condition, $H_{y_x}, H_{y_z}, E_{x_z}$ and E_{z_x}, has been used. In order to derive the wave equation for the TM polarization, we substitute (4) in (6) and (5) in (7), to obtain

$$-\omega^2\mu\epsilon H_{y_x} = \frac{1}{s_x}\frac{\partial}{\partial x}\frac{1}{s_x}\frac{\partial}{\partial x}H_y \tag{8}$$

$$-\omega^2\mu\epsilon H_{y_z} = \frac{1}{s_z}\frac{\partial}{\partial z}\frac{1}{s_z}\frac{\partial}{\partial z}H_y. \tag{9}$$

Since $(H_{y_x} + H_{y_z}) = H_y$ we obtain

$$-\omega^2\mu\epsilon H_y = \frac{1}{s_x}\frac{\partial}{\partial x}\frac{1}{s_x}\frac{\partial}{\partial x}H_y + \frac{1}{s_z}\frac{\partial}{\partial z}\frac{1}{s_z}\frac{\partial}{\partial z}H_y. \tag{10}$$

Next, we consider the eigenvalue problem associated with the TM-modes of the slab dielectric waveguide shown in Fig. 1. Nonmagnetic materials are assumed. The waveguide has thickness $2w$, constant permittivity ϵ_1, and its axis coincides with the z axis. Due to the symmetry of the structure, only the top half is shown. A slab of thickness l and permittivity $\epsilon_2 < \epsilon_1$ represents the medium outside the guide. Notice that $s_x = s_z = s = 1$ for both the guide and the adjacent slab. Beyond the ϵ_2 slab we introduced an M-layer structure terminated by a perfect magnetic conductor. All layers in the structure have the same permittivity, ϵ_2; however, their thicknesses, d_i, and the values of s_{x_i}, are allowed to vary, while $s_{z_i} = 1, i = 1, 2, \cdots, M$. Let β be the unknown propagation constant for even TM-mode propagation in z. A straightforward analysis of the eigenvalue problem results in the following eigenvalue equation

$$\tan(k_{x_1}w) = \frac{k_{x_2}\epsilon_1}{k_{x_1}\epsilon_2} \times \mathcal{E} \tag{11}$$

where $\mathcal{E}$ is given by

$$\mathcal{E} = \frac{1 + \exp\left(-2k_{x_2}l\right)\exp\left(-2k_{x_2}\sum_{i=1}^{M} s_{x_i}d_i\right)}{1 - \exp\left(-2k_{x_2}l\right)\exp\left(-2k_{x_2}\sum_{i=1}^{M} s_{x_i}d_i\right)} \tag{12}$$

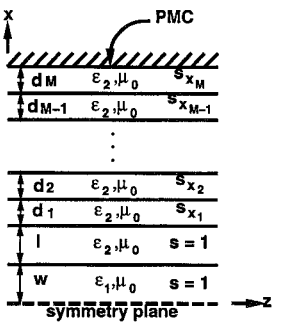

Fig. 1. Slab waveguide geometry for analytically soluble problem.

with $k_{x_1}^2 = \omega^2\mu_0\epsilon_1 - \beta^2$ and $k_{x_2}^2 = \beta^2 - \omega^2\mu_0\epsilon_2$. For propagating modes, k_{x_2} is real and positive. At this point, it is appropriate to recall that the eigenvalue equation for the even TM modes for the case of the standard slab waveguide of thickness $2w$ and permittivity ϵ_1 embedded in a homogeneous medium ϵ_2 is given by

$$\tan(k_1 w) = (k_2\epsilon_1)/(k_1\epsilon_2).$$

Thus, the term $\mathcal{E}$ of (12) may be thought of as the "error" term caused by the truncated domain and the presence of the layered structure. It can be seen that as $l \to \infty$ in (12), $\mathcal{E} \to 1$, recovering the eigenvalue equation for the standard slab waveguide. Equation (12) also suggests that instead of letting $l \to \infty$, the eigenvalue equation for the standard waveguide can be reclaimed by letting s_{x_i} assume large real values. We notice that s_{x_i} needs to be real and positive to cause the error terms to become negligible compared to 1. Recall that for Berenger's PML s_{x_i} is of the form $s_{x_i} = 1 - j(\sigma_i/\omega\epsilon_i)$ and, as such, it does not cause any additional attenuation (since k_{x_2} is real) to help reduce the error term in (11).

III. Numerical Implementation

The analysis of the previous section suggests the use of s values with $\mathrm{Re}\{s\} > 1$ in order to facilitate rapid absorption of evanescent waves without affecting their propagation characteristics. Indeed, it is shown in [4] that

$$s = s' - js''$$

is the general solution for the stretching parameter which gives a reflectionless interface. Therefore, in order to encompass the general case of planar structures that have both radiating and waveguiding properties, we allow s to assume complex values with a real part greater than 1. More specifically, s_i takes the form

$$s_i = s_i' - js_i'' = s_i'\left(1 - j\frac{s_i''}{s_i'}\right) = s_i'\left(1 - j\frac{\sigma_i}{\omega\epsilon}\right) \tag{13}$$

where $i = x, y, z$. By factoring out the s_i' term, the standard PML imaginary part $\sigma/(\omega\epsilon)$ is given by s_i''/s_i'. This formalism was selected because it facilitates a straightforward implementation of the modified PML in the time-dependent Maxwell's equations that reduces to the orginal Berenger's PML formalism when $s_i' = 1$.

With this notation for s_i, the modified Maxwell's system for the TM case, (4)–(7), takes the form

$$\left(\epsilon\frac{\partial}{\partial t} + \sigma_x\right)E_z = \frac{1}{s_x'}\frac{\partial}{\partial x}(H_{y_x} + H_{y_z}) \tag{14}$$

$$\left(\epsilon\frac{\partial}{\partial t} + \sigma_z\right)E_x = -\frac{1}{s_z'}\frac{\partial}{\partial z}(H_{y_x} + H_{y_z}) \tag{15}$$

$$\left(\mu\frac{\partial}{\partial t} + \frac{\sigma_x\mu}{\epsilon}\right)H_{y_x} = \frac{1}{s_x'}\frac{\partial}{\partial x}E_z \tag{16}$$

$$\left(\mu\frac{\partial}{\partial t} + \frac{\sigma_z\mu}{\epsilon}\right)H_{y_z} = -\frac{1}{s_z'}\frac{\partial}{\partial z}E_x. \tag{17}$$

In the above equations the PML condition $\sigma_i/\epsilon = \sigma_i^*/\mu, i = x, z$ has been used in order to express the magnetic conductivity σ_i^* in terms of the electric conductivity σ_i. Clearly, the numerical implementation of the standard Berenger PML is recovered by setting $s_i' = 1$ $(i = x, z)$. The extension to three dimensions is straightforward

$$\left(\epsilon\frac{\partial}{\partial t} + \sigma_y\right)E_{x_y} = \frac{1}{s_y'}\frac{\partial}{\partial y}(H_{z_x} + H_{z_y}) \tag{18}$$

$$\left(\epsilon\frac{\partial}{\partial t} + \sigma_z\right)E_{x_z} = -\frac{1}{s_z'}\frac{\partial}{\partial z}(H_{y_x} + H_{y_z}) \tag{19}$$

$$\left(\epsilon\frac{\partial}{\partial t} + \sigma_x\right)E_{y_x} = -\frac{1}{s_x'}\frac{\partial}{\partial x}(H_{z_x} + H_{z_y}) \tag{20}$$

$$\left(\epsilon\frac{\partial}{\partial t} + \sigma_z\right)E_{y_z} = \frac{1}{s_z'}\frac{\partial}{\partial z}(H_{x_y} + H_{x_z}) \tag{21}$$

$$\left(\epsilon\frac{\partial}{\partial t} + \sigma_x\right)E_{z_x} = \frac{1}{s_x'}\frac{\partial}{\partial x}(H_{y_x} + H_{y_z}) \tag{22}$$

$$\left(\epsilon\frac{\partial}{\partial t} + \sigma_y\right)E_{z_y} = -\frac{1}{s_y'}\frac{\partial}{\partial y}(H_{x_y} + H_{x_z}) \tag{23}$$

$$\left(\mu\frac{\partial}{\partial t} + \frac{\sigma_y\mu}{\epsilon}\right)H_{x_y} = -\frac{1}{s_y'}\frac{\partial}{\partial y}(E_{z_x} + E_{z_y}) \tag{24}$$

$$\left(\mu\frac{\partial}{\partial t} + \frac{\sigma_z\mu}{\epsilon}\right)H_{x_z} = \frac{1}{s_z'}\frac{\partial}{\partial z}(E_{y_x} + E_{y_z}) \tag{25}$$

$$\left(\mu\frac{\partial}{\partial t} + \frac{\sigma_x\mu}{\epsilon}\right)H_{y_x} = \frac{1}{s_x'}\frac{\partial}{\partial x}(E_{z_x} + E_{z_y}) \tag{26}$$

$$\left(\mu\frac{\partial}{\partial t} + \frac{\sigma_z\mu}{\epsilon}\right)H_{y_z} = -\frac{1}{s_z'}\frac{\partial}{\partial z}(E_{x_y} + E_{x_z}) \tag{27}$$

$$\left(\mu\frac{\partial}{\partial t} + \frac{\sigma_x\mu}{\epsilon}\right)H_{z_x} = -\frac{1}{s_x'}\frac{\partial}{\partial x}(E_{y_x} + E_{y_z}) \tag{28}$$

$$\left(\mu\frac{\partial}{\partial t} + \frac{\sigma_y\mu}{\epsilon}\right)H_{z_y} = \frac{1}{s_y'}\frac{\partial}{\partial y}(E_{x_y} + E_{x_z}). \tag{29}$$

This analysis can also be applied in a straightforward manner to compact 2D-FDTD simulations for the dispersive analysis of uniform waveguiding structures [5]. Let z be the axis of the uniform waveguide. Using (3) and assuming propagation in z of the form $\exp(-j\beta z)$, Maxwell's curl equations become

$$\epsilon\frac{\partial}{\partial t}E_x = \frac{1}{s_y}\frac{\partial}{\partial y}H_z + j\beta H_y \tag{30}$$

$$\epsilon\frac{\partial}{\partial t}E_y = -j\beta H_x - \frac{1}{s_x}\frac{\partial}{\partial x}H_z \tag{31}$$

$$\epsilon\frac{\partial}{\partial t}E_z = \frac{1}{s_x}\frac{\partial}{\partial x}H_y - \frac{1}{s_y}\frac{\partial}{\partial y}H_x \tag{32}$$

$$\mu\frac{\partial}{\partial t}H_x = -\frac{1}{s_y}\frac{\partial}{\partial y}E_z - j\beta E_y \tag{33}$$

$$\mu\frac{\partial}{\partial t}H_y = j\beta E_x + \frac{1}{s_x}\frac{\partial}{\partial x}E_z \tag{34}$$

$$\mu\frac{\partial}{\partial t}H_z = -\frac{1}{s_x}\frac{\partial}{\partial x}E_y + \frac{1}{s_y}\frac{\partial}{\partial y}E_x \tag{35}$$

where s_x and s_y are of the form in (13). If only lossless systems (i.e., planar waveguides that do not support leaky modes) are considered, then the field profiles in the transverse plane will be purely evanescent. Therefore, the σ_i in (13) can be set to zero, resulting in $s_i = s_i'$. This result shows that evanescent waves can be absorbed in the PML by simply scaling the directional derivatives with factors of $1/s_i$ where $i = x, y$. Also, since $\sigma_i \equiv 0$, exponential differencing and splitting of the field components are not required. This means that absorption of purely evanescent fields can be accounted for in existing compact 2D-FDTD codes with very little modification.

IV. Numerical Studies

First, we consider the slab dielectric waveguide of Fig. 1. The core has a half width $w = 0.5$ cm and index of refraction of 1.3 and is surrounded by air. A free space operating wavelength of $\lambda = 3.0$ cm is assumed in order to ensure single mode propagation. Also, the analytic solution for the effective index is $n_{\text{eff}} = 1.0794$ which is near cutoff implying a mode with significant energy in the evanescent tails. For the numerical implementation, 5 cells were used between the core and the PML. For the discretization of $dx = dy = 1.0$ mm used, this corresponds to $l = 0.5$ cm. The PML is 10 cells thick and parabolically graded with the real part of s_{x_i} varied as

$$s_{x_i} = (s_{\max} - 1)\left(\frac{i}{10}\right)^2 + 1 \qquad i = 1, 2, \cdots, 10. \tag{36}$$

For this parabolic variation, the average value of s_i, s_{avg}, is related to $s_{\max}$ in the following manner

$$s_{\max} = 3s_{\text{avg}} - 2. \tag{37}$$

Fig. 2 shows the analytic results of (11) with $s = s_i'$ (solid line), i.e. $\sigma = 0$, compared with FDTD numerical results (*) versus s_{avg}. The dotted line is the result of (11) with $\mathcal{E} = 1$. The stars are obtained from the numerical implementation of (14)–(17). For these results we excited the structure with the proper mode driven at the frequency of interest, with σ set to zero. We see that the trend of the numerical implementation matches that of the analytic results. Furthermore, in all cases

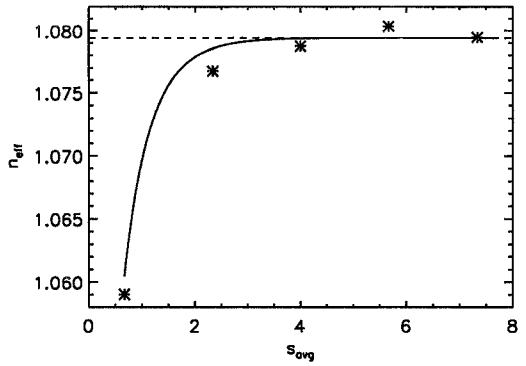

Fig. 2. Results for slab waveguide problem (- - - solution of (11) with $\mathcal{E} = 1$, — solution of (11) with $\sigma = 0$, $*$ FDTD results).

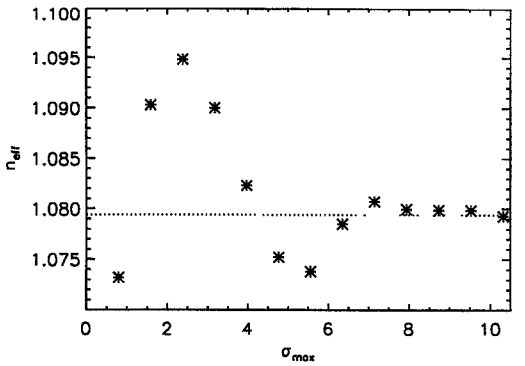

Fig. 3. Results for slab waveguide problem, n_{eff} as a function of $\sigma_{\max}$ with $s_{\text{avg}} = 1$. (- - - solution of (11) with $\mathcal{E} = 1$, $*$ FDTD results).

the percent difference between the analytical and numerical results is less than 0.5%. We note that the magnitude of the normalized modal field at the PML interface is around 0.46, showing that it is not necessary to let the field decay significantly before introducing the PML.

For a more rigorous test, instead of exciting the guide with a modal field, we excited the guide with a Gaussian profile driven at the frequency of interest. Specifically, we used

$$H_y(x,t) \simeq \exp\left[-\left(\frac{2x}{w}\right)^2\right] \sin(2\pi c_0 t/\lambda_0)$$

where w is the core half width, c_0 is the speed of light in vacuum, and λ_0 is the free space wavelength of interest. This excitation is highly concentrated in the core region of the waveguide. This implies that there will be significant energy radiating from this aperature excitation away from the guide which needs to be absorbed, in addition to the evanescent field of the waveguide mode.

In Fig. 3, we attempted to find the effective index of the mode utilizing a parabolically graded σ only, i.e., $s_{\text{avg}} = 1$ and $\sigma = \sigma_{\max}(i/M)^2$. In other words, we attempted the solution of the eigenvaule problem using the original PML formalism. The value of $\sigma_{\max}$ was chosen by the formula

$$\sigma_{\max} = \frac{q\ \ln(10)\epsilon c_0 M^2}{2\ dx \sum_{i=1}^{M} i^2}$$

where q is the desired order of the reflection coefficent. This is nothing more than a discrete form of the equation proposed by Berenger [1]. We see that the value of n_{eff} is highly oscillatory as a function of $\sigma_{\max}$. It is believed that this is due to the evanescent field not being properly accounted for. However, as $\sigma_{\max}$ increases, n_{eff} does approach the correct value. While this result is not clearly understood at the time this paper is written, it is believed to be the result of some resonance phenomenon attributed to the phase term $\exp(-j\sigma k_{x_2}/\omega\epsilon)$ introduced by the PML.

The results of Fig. 3 should be contrasted to Fig. 4. In Fig. 4, $\sigma_{\max}$ is kept constant at 3.175 $(1/\Omega$ m), while s_{avg} is varied. Referrring to Fig. 3, we see that this value of $\sigma_{\max}$ with $s_{\text{avg}} = 1$ results in $n_{\text{eff}} = 1.09$. By using an s_{avg} of greater than 2.0, we see a dramatic improvement in the value of n_{eff}.

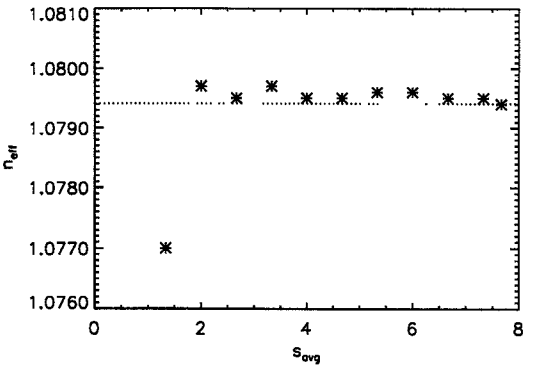

Fig. 4. Results for slab waveguide problem, n_{eff} as a function of s_{avg} with $\sigma_{\max} = 3.175$ $(1/\Omega$ m). (- - - solution of (11) with $\mathcal{E} = 1$, $*$ FDTD results).

We see that in Fig. 4, n_{eff} does have an oscillatory behavior as in Fig. 3, however the oscillations are much smaller and the obtained n_{eff} values are in excellent agreement with the analytical value of n_{eff} over most of the range, in direct constrast to the results in Fig. 3.

As another application of this modified PML truncation scheme consider the compact 2D-FDTD dispersion analysis of open multiconductor waveguiding systems [5]. Comparisons with other methods for both microstrip and coupled microstrip structures will be made. Fig. 5 shows the different regions of interest for compact 2D-FDTD implementations of these problems. Region 1 represents the FDTD domain and regions 2–4 show the PML's. For these specific applications, we are interested in propagating modes only. For such cases, since there is no splitting of the field components, the same update equations for the field components may be used in both the FDTD and PML regions.

The insert in Fig. 6 shows the geometry for an unshielded microstrip line where $w = 1$ cm, $h = 1$ cm, $\epsilon_1 = 2.1\epsilon_0, \beta = 2.0$ $(1/\text{cm})$, with the PML positioned 5 cells away from the conductor strip. The PML is made up of 10 cells on the left, top, and right sides. A parabolic variation in s is used. The reference solution for the effective dielectric constant, $\epsilon_{r,\text{eff}}$, of the microstrip is given by Kirchning and Jansen [6] and was determined by functional approximations from theoretical and measured values. The values obtained by these functional approximations have errors for $\epsilon_{r,\text{eff}}$ less than 0.6% for $0.1 \leq$

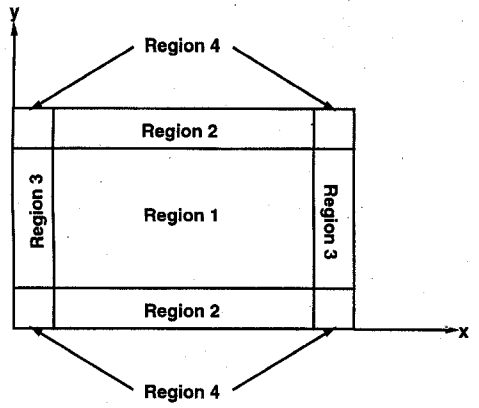

Fig. 5. Placement of modified PML regions for 2D-FDTD grid truncation.

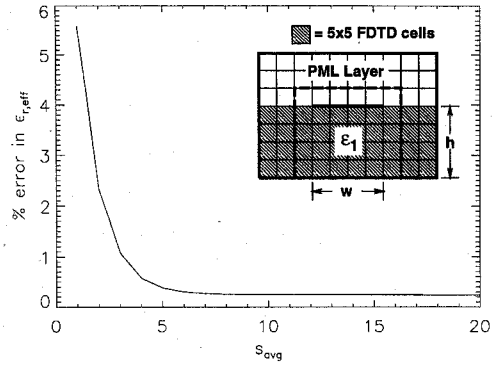

Fig. 6. Percent error in effective permittivity of an unshielded microstrip with $w = h = 1$ cm, $\epsilon_1 = 2.1\epsilon_0$, $\beta = 2.0$ cm^{-1}. 10 cell thick PML's with parabolic variation in s are placed 10 cells away from the strip.

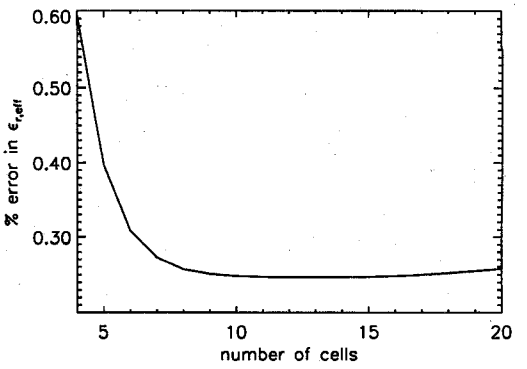

Fig. 7. Percent error in effective permittivity of the microstrip of Fig. 6 versus number of cells in PML. The variation in s is parabolic with $s_{\text{avg}} = 10$. The PML's are placed 10 cells away from the strip.

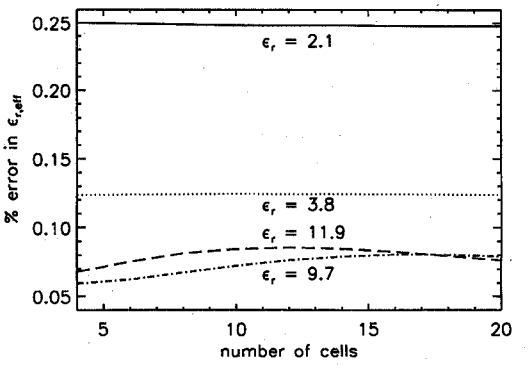

Fig. 8. Percent error in effective permittivity of a microstrip versus number of cells in the buffer layer between conductor and PML for different values of ϵ_r. A parabolic variation in s with $s_{\text{avg}} = 10$ is used. The PML's are 10 cells thick.

$w/h \leq 100$ with $1 \leq \epsilon_r \leq 20$ and $0 \leq h/\lambda_0 \leq 0.13$. Fig. 6 plots the percent error of the compact 2D-FDTD solution for $\epsilon_{r,\text{eff}}$ as the value of s_{avg} in s_x and s_y changes. For values of $s_{\text{avg}} \geq 4$, the accuracy of the FDTD solution is within the accuracy of the reference solution. Fig. 7 shows the effect of varying the number of cells in the PML for the same microstrip geometry as in Fig. 6. The variation in s is parabolic with $s_{\text{avg}} = 10$. This plot shows that very accurate values for $\epsilon_{r,\text{eff}}$ can be obtained with as little as 4 cells in the PML.

Next, the accuracy of $\epsilon_{r,\text{eff}}$ for the unshielded microstrip is examined when the number of cells in the buffer region between the conductor and PML is varied for different values of ϵ_r and w. Fig. 8 shows how the percent error in $\epsilon_{r,\text{eff}}$ changes as the number of cells in the buffer region increases from 4–20, for different values of ϵ_r with $w = 1$ cm, $h = 1$ cm, and $\beta = 2.0$ (1/cm). The PML is made up of 10 cells on the left, top, and right sides. Once again, a parabolic variation of s in the PML with $s_{\text{avg}} = 10$ is used. A general trend which can be observed is that the accuracy of the calculated value of $\epsilon_{r,\text{eff}}$ increases with larger values of ϵ_r. This is consistent with the fact that microstrip structures with lower values of substrate dielectric constant exhibit stronger fringing. The anomalous behavior in the percent error value depicted in Fig. 8 for large values of ϵ_r could be due to the error in the reference solution since the FDTD results are well within the accuracy of the reference.

Fig. 9 shows how the error in the calculated value of $\epsilon_{r,\text{eff}}$ changes for different values of w with all other parameters being the same as those for Fig. 6 with $s_{\text{avg}} = 10$. This study shows that as the width of the conductor decreases, the error in $\epsilon_{r,\text{eff}}$ increases. Again, this behavior is consistent with the fact that the fringing of the field is more profound for lower values of w/h. Clearly, the smaller the ratio w/h, the larger the distance between the PML and the conductor need be, even though the dependence is negligible for $w/h > 0.6$. Once again, since the FDTD solution is within the accuracy of the reference solution for larger values of w/h, no comments can be made about the general behavior for these cases, except that the error in $\epsilon_{r,\text{eff}}$ is clearly less than that for microstrips with small values of w/h (<0.5). This study was done for a substrate with $\epsilon_r = 2.1$. In view of the fact that larger values of ϵ_r reduce fringing, this study suggests that the modified PML can be placed as close as 5 cells away from the strips for microstrip structures with $w/h > 0.3$ and $\epsilon_r > 2$. Furthermore, the results in the previous figures indicate that a 5-cell modified PML with $s_{\text{avg}} = 5$ suffices for highly accurate compact 2D-FDTD dispersion analysis of unshielded microstrip structures.

The next study considers the compact 2D-FDTD analysis of a coupled microstrip structure. Fig. 10 depicts the frequency dependence of the effective dielectric constant for the even and odd modes of the coupled microstrip shown in the insert

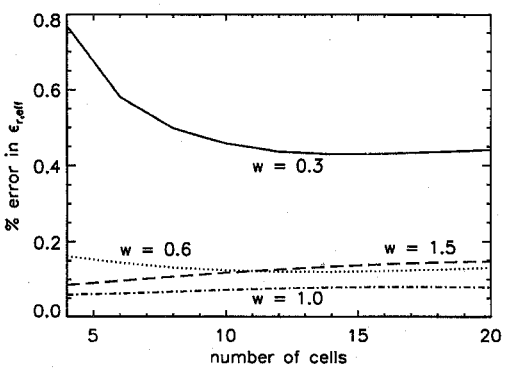

Fig. 9. Percent error in effective permittivity of a microstrip versus number of cells in the buffer layer between conductor and PML for different values of w. 10 cell thick PML's with parabolic variation in s ($s_{\text{avg}} = 10$) are used.

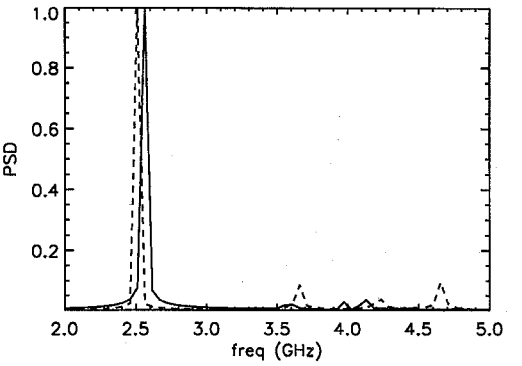

Fig. 11. Power spectral density of odd mode for the coupled microstrip shown in the insert in Fig. 10. (— modified PML boundary condition, --- PMC/PEC boundary condition).

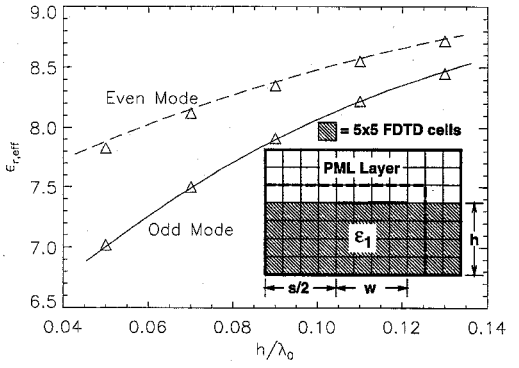

Fig. 10. Effective permittivity of even and odd mode for a coupled microstrip (— and --- 2D-FDTD results, △ results from [6]). 10 cell thick PML's with parabolic variation in s ($s_{\text{avg}} = 10$) are placed 5 cells away from the conductor.

obtained from a compact 2D-FDTD simulation with modified PML truncation. For this specific geometry, $w/h = 1, s/h = 2$, and $\epsilon_1 = 9.7\epsilon_0$. For the odd mode, perfect electric conductor (PEC) walls are placed on the left and bottom sides while 10 cell parabolic PML's ($s_{\text{avg}} = 10$) are placed on the top and right sides. The even mode is modeled in a similar fashion, except that the PEC on the left wall is replaced with a perfect magnetic conductor (PMC). Even though for both cases the modified PML layers are placed only 5 cells from the conductor, the agreement with the results in [6] (△) is within 1.25%. However, it is important to point out that the accuracy of the results in [6] is not known.

Finally, in order to provide an additional demonstration of the effectiveness of the modified PMLs, a comparison was made to the case with the PML absent. The structure under study is the aforementioned symmetric coupled microstrip. Fifteen cells from the conductor, a PEC is placed on the top side and a PMC is placed on the right side. This choice of top and right walls is not arbitrary. The PEC at the top is based on the assumption that the tangential electric field is negligible at that distance from the strip. The PMC on the right is based on the assumption that, in that direction, the electric field is essentially parallel to the wall sufficently far away from the strip. Fig. 11 shows the power spectral densities (PSD) of the transformed time domain responses for the odd mode with $\beta = 1.5$ (1/cm). The solid and dashed lines denote the spectrum obtained by using the modified PML and PEC/PMC boundary conditions respectively. The shift in frequency for the PEC/PMC boundary condition translates to an 8% error in $\epsilon_{r,\text{eff}}$. Also note that the PSD for this case shows appreciable energy beyond the fundamental mode. This is due to excitation of higher order (waveguide) modes in the structure caused by the presence of the PEC/PMC walls.

V. Conclusion

This paper has demonstrated that, in its original form, the Berenger PML grid truncation scheme yields unpredictable results when applied to waveguiding structures that support bound waves with evanescent behavior. A modification to the original PML has been introduced which overcomes this limitation and provides for numerical solutions of high accuracy. Analytic and numerical studies of the symmetric slab waveguide demonstrated that the modified PML reduces the sensitivity of the calculated eigenvalue to the selection of the conductivities of the PML. An interesting application of the proposed modified PML to grid truncation for compact 2D-FDTD simulations was presented. Numerical studies of single and coupled microstrip structures demonstrated that the modified PML was very effective in truncating the purely evanescent fields associated with the propagating modes in such planar waveguides, thus allowing for a highly accurate and computationally efficent dispersion analysis. More important, it was shown that if the analysis is restricted only to propagating (non-leaky) modes, the modified PML does not require field splitting and its numerical implementation is very straightforward.

References

[1] J. P. Berenger, "A perfectly matched layer for the absorption of electromagnetic waves," *J. Computational Physics,* vol. 114, pp. 185–200, 1994.

[2] ——, "A perfectly matched layer for free-space simulation in finite-difference computer codes," submitted to *Annales des Télécommunications,* preprint 1994.

[3] C. E. Reuter, R. M. Joseph, E. T. Thiele, D. S. Katz, and A. Taflove, "Ultrawideband absorbing boundary condition for termination of waveguiding structures in FD-TD simulations," *IEEE Microwave and Guided Wave Lett.,* vol. 4, pp. 344–346, Oct. 1994.

[4] W. C. Chew and W. H. Weedon, "A 3-D perfectly matched medium from modified Maxwell's equations with stretched coordinates," *Microwave and Optical Tech. Lett.,* vol. 7, pp. 599–604, Sept. 1994.
[5] S. Xiao, R. Vahldieck, and H. Jin, "Full-wave analysis of guided wave structures using a novel 2-D FDTD," *IEEE Microwave and Guided Wave Lett.,* vol. 2, pp. 165–167, May 1994.
[6] R. K. Hoffman, *Handbook of Microwave Integrated Circuits.* Norwood, MA: Artech House, 1987, pp. 167–174 and 245–247.

Michael A. Gribbons received the B.S. degree in electrical engineering from the University of Illinois, Urbana, in 1989. He completed the M.S. degree in electrical engineering in 1993 and is currently working towards a Ph.D. degree, both at the University of Arizona, Tucson.

Currently, he is a Graduate Research Associate at the University of Arizona with research interests in the analysis of optical waveguides and the development of numerical tools for the design of optical interconnects.

William P. Pinello received the B.S.E.E. from Ohio State University, Columbus in 1992. He is presently working toward the M.S. degree in electrical engineering and is a Research Assistant in the Center for Electronic Packaging Research at the University of Arizona, Tucson.

His research interests are in the electromagnetic modeling of high-frequency electrical and optical interconnections.

Andreas C. Cangellaris (M'86) received the Diploma in electrical engineering from the Aristotelian University of Thessaloniki, Greece, in 1981, and the M.S. and Ph.D. degrees in electrical engineering from the University of California, Berekley in 1983 and 1985, respectively.

From 1985 to 1987, he was with the Electronics Department at General Motors Research Laboratories in Warren, MI. In 1987, he joined the Department of Electrical and Computer Engineering at the University of Arizona, where he is currently Associate Professor. His current research interests are in computational and applied electromagnetics, RF and microwave circuits, and the development of electromagnetic software tools for electrical analysis and design of packaged digital and analog electronic systems with emphasis on electromagnetic effects and electromagnetic compatibility.